JACS
JOURNAL OF THE AMERICAN CHEMICAL SOCIETY
Article
pubs.acs.org/JACS

Free Radical Coupling of *o*-Semiquinones Uncovered

Alessandro Pezzella,[†] Orlando Crescenzi,[†] Lucia Panzella,[†] Alessandra Napolitano,[†] Edward J. Land,[‡,§] Vincenzo Barone,*[,∥] and Marco d'Ischia*[,†]

[†]Department of Chemical Sciences, University of Naples Federico II, Via Cintia 4, I-80126 Naples, Italy
[‡]STFC Daresbury Laboratory, Daresbury, WA4 4AD, United Kingdom
[§]Chemistry Section, School of Physical and Geographical Sciences, Keele University, Staffs ST5 5BG, United Kingdom
[∥]Scuola Normale Superiore, Piazza dei Cavalieri 7, I-56126 Pisa, Italy

Supporting Information

ABSTRACT: As a rule, *o*-semiquinones decay through disproportionation leading to equimolar amounts of catechol and *o*-quinone products. However, the *o*-semiquinone **1S** generated by pulse radiolysis oxidation of the eumelanin precursor 5,6-dihydroxyindole (**1**) decays with second-order kinetics to generate broad visible chromophores that are incompatible with the predicted absorption of 5,6-indolequinone (**1Q**). Using an integrated chemical, pulse radiolytic and computational approach as well as deuterium labeling, we show herein that **1S** and related 5,6-dihydroxyindole semiquinones decay mainly by a free radical coupling mechanism. This conclusion was supported by the inverse kinetic isotope effect observed with deuterated **1S**, the identification of unprecedented dihydrobiindole products by one-electron oxidation of **1**, the good matching of simulated absorption profiles of free radical coupling products of **1S** with experimental spectra, and a detailed computational analysis of the kinetics and thermodynamics of the disproportionation equilibrium and free radical coupling of **1S** versus **1**-**1Q** coupling. These results disclose, to the best of our knowledge, the first example of free radical dimerization of *o*-semiquinones outcompeting the classic disproportionation-driven catechol-quinone coupling and suggest that this hitherto unrecognized process may be of broader relevance than previously believed.

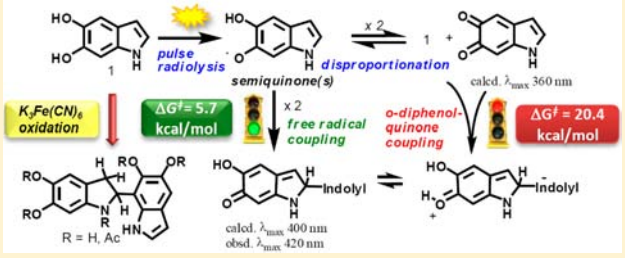

INTRODUCTION

Semiquinones ($QH^{\bullet}$) can be detected as labile intermediates in the redox transformations of quinones (Q) and *o*-/*p*-diphenols (QH_2) and are involved in a variety of important processes of biological, pharmacological, and toxicological relevance.[1−4] The fate of semiquinones depends on a number of factors including the thermodynamic parameters controlling the equilibria in which these species are involved and the chemical characteristics of the reaction environment (solvent dielectric constant, presence of metal ions, etc.). In the absence of redox active systems and radical quenching pathways, disproportionation is widely recognized as the favored pathway of semiquinone decay in water at pH around neutrality:

$$2QH^{\bullet} \rightarrow QH_2 + Q \quad (1)$$

In some cases the thermodynamic parameters controlling the disproportionation of semiquinones have been determined by EPR-based approaches.[1] However, considerable gaps persist in those cases where EPR techniques fail to provide a satisfactory characterization of semiquinones due to their marked instability. A typical case in point is represented by 5,6-dihydroxyindole (**1**) and its 2-carboxylic acid (**2**), naturally occurring tyrosine metabolites which can undergo oxidative polymerization via a range of oligomer intermediates[5−10] to give the black insoluble eumelanin pigments of skin, hair, and eyes.[11−13] Interest in eumelanin and the underlying biosynthetic pathway has traditionally been spurred by the central relevance to human pigmentation and related disorders, including melanoma etiopathogenesis and treatment.[14] During the past decade, however, eumelanins have attracted increasing attention within the materials science community in view of their unique physical properties and supramolecular organization suggesting application as soft, biocompatible, and tailorable functional materials for organoelectronics.[15,16] Although eumelanins exhibit both intrinsic and inducible free radical character,[17] attempts to detect and characterize semiquinone intermediates in the oxidative polymerization of 5,6-dihydroxyindoles by means of EPR investigations have been largely unsuccessful. Whether these semiquinones can be converted to 5,6-indolequinones and by what mechanism is also an open issue. These latter quinones, which resemble the elusive 2,3-naphthoquinones, are highly unstable species because of the incompatibility of the dione moiety at the 5,6-positions with the aromaticity of the pyrrole ring.[18] As a consequence, their structural and chemical characterization has remained a formidable challenge. Even the spectroscopic properties of 5,6-indolequinones have long been a matter of

Received: July 3, 2013
Published: July 17, 2013

   dx.doi.org/10.1021/ja4067332 | J. Am. Chem. Soc. 2013, 135, 12142−12149

controversy, to the point that their actual existence as independent intermediates in the oxidation of 5,6-dihydroxyindoles to eumelanin has been questioned.[18]

Valuable insights into 5,6-dihydroxyindole oxidation mechanism have derived from pulse radiolysis studies.[18−20] One-electron oxidation of **1** in aqueous solution at pH 7.4 was found to produce an initial spectrum with peaks at 330 and 490 nm and a shoulder at 360 nm,[19] attributed to the semiquinone **1S**. Decay of **1S** follows second-order kinetics and leads to the formation of a distinct chromophore absorbing in the range 400−430 nm, originally identified as 5,6-indolequinone (**1Q-I**) produced by a disproportionation process (Scheme 1). It was suggested, in particular, that the *o*-quinone **1Q-I**, as generated, rapidly isomerizes to the quinone methide (**1Q-II**) and quinoneimine (**1Q-III**) tautomers.

Scheme 1. Isomeric Semiquinone (S) and 5,6-Indolequinone (Q) Species Produced by One-Electron Oxidation of 5,6-Dihydroxyindoles 1−3

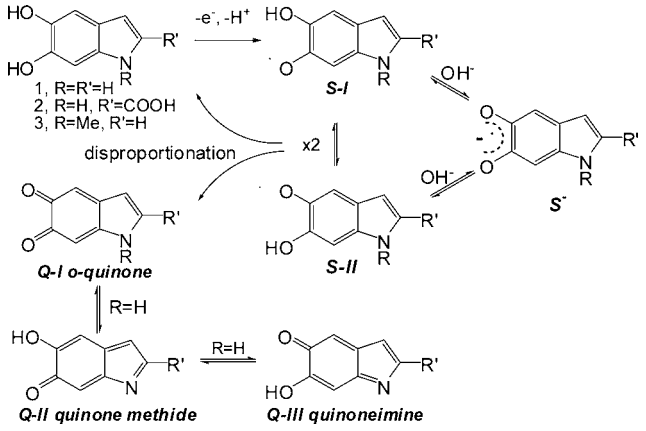

The actual importance of tautomerism and isomer equilibration processes for 5,6-indolequinones is however open to question based on the finding that 5,6-dihydroxy-1-methylindole (**3**) exhibits a pulse radiolysis behavior akin to that of **1**.[19] Since conversion of the *o*-quinone to quinone methide and quinonimine tautomers in **3** would be hindered by the *N*-methyl substituent, it can be argued that **1** and **3** generate semiquinones that decay by similar pathways. Pulse radiolytic oxidation of **2** showed the formation of a similar semiquinone which decayed with second-order kinetics leading to unexpectedly weak visible chromophores, reflecting evidently the influence of the carboxyl group on the nature and/or the absorption features of the products.[7]

A most intriguing observation, however, that further compounded the issue, came from a DFT investigation of the vertical excitation energies and calculated absorption spectra for all tautomers of **1** and **1Q**.[21] Predicted absorption maxima of quinone tautomers **1QI−III** were found to fall out of the 400−600 nm range, which raised doubts on the proposed generation of 5,6-indolequinones by disproportionation of **1S**.

Because of the central relevance of 5,6-dihydroxyindole oxidation chemistry to eumelanin synthesis and applications, we were prompted to re-examine the mechanism and products of semiquinone decay by an integrated chemical-pulse radiolytic-DFT approach using deuterium labeling as a mechanistic probe. Specific aims of the study were: (a) to determine the effects of site specific deuteration on the kinetics of decay of **1S**, as a means of gauging isotope-sensitive pathways; (b) to assess the energetics of disproportionation equilibria and the effects of substituents for 5,6-dihydroxyindole-derived semiquinones; (c) to characterize the main intermediates and isolable products in the coupling process; and (d) to assess the free energy changes and transition-state barriers for the various coupling pathways.

RESULTS AND DISCUSSION

Experiment Design and Synthesis of Deuterated Derivatives. For the aim of the present study, 5,6-dihydroxyindoles **1**−**3** were selected as substrates both for their relevance to eumelanin synthesis and their patterns of substitution, expected to provide useful mechanistic information. Deuterated derivatives of **1** were also identified as useful synthetic targets since deuterium substitution would allow to probe the involvement of putative reaction sites during oxidative processes by measuring kinetic isotope effects (Scheme 2). Since straightforward procedures for preparing deuterium-labeled 5,6-dihydroxyindoles were lacking, concise expedient approaches for the purposes of this study were devised. All the deuterium-labeled compounds and, more in general, all substrates prepared in this study were obtained as the *O*-acetylated derivatives[5,18] due to the notorious instability of 5,6-dihydroxyindoles to oxidation. 5,6-Diacetoxyindoles are commonly used as storable and ready sources of 5,6-dihydroxyindoles because they can be easily hydrolyzed in situ under mild conditions to provide the parent catecholic compounds, thus eliminating the need to deal with the unstable *o*-diphenol.

Scheme 2. Synthetic Approaches to Deuterated 1[a]

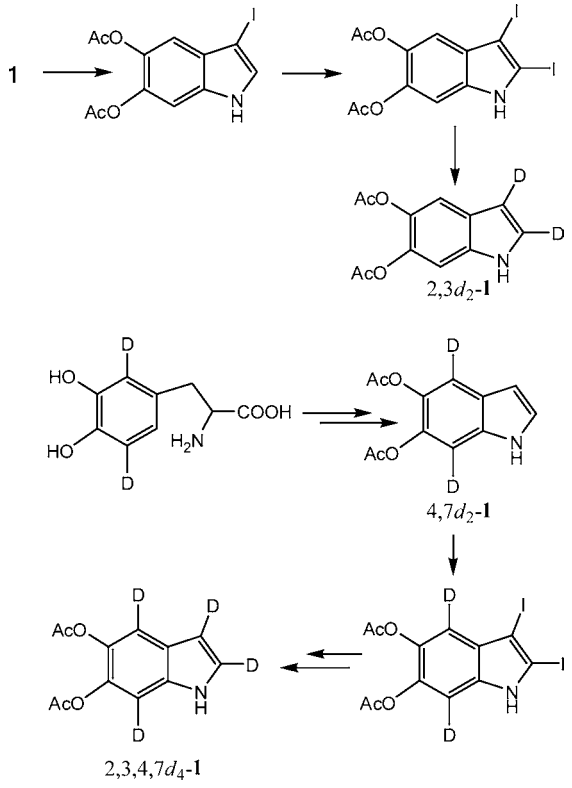

[a]Details of reagents and conditions are provided in Supporting Information.

dx.doi.org/10.1021/ja4067332 | J. Am. Chem. Soc. 2013, 135, 12142−12149

Deuteration at the 3- and 2- positions of **1** could be easily achieved via reduction of the appropriate iodo derivatives with Zn in CD_3COOD. Capitalizing on the recently reported syntheses of 5,6-diacetoxy-3-iodoindole and 5,6-diacetoxy-2,3-diiodoindole,[22,23] this procedure was successfully applied to the preparation of the labeled derivative 2,3d_2-**1** in satisfactory yields. Small amounts of the 4,7-dideutero derivative of **1** were prepared by a related biomimetic procedures involving oxidation of commercially available 2,5,6-trideuteroDOPA.[24] Finally, 2,3,4,7d_4-**1** was prepared by double iodination of the 4,7-dideutero derivative[22] followed by reductive displacement of the halogens with deuterium as above. Isotopic purity analysis by NMR indicated that residual H percentage at each deuterated position did not exceed 5% (Supporting Information, SI).

Since use of deuterated 5,6-dihydroxyindoles as mechanistic probes requires that the compounds firmly retain deuterium under the various conditions of the pulse radiolysis experiments, including acetyl group removal and incubation at pH 7.4, isotope retention in deuterated 5,6-dihydroxyindoles was preliminarily investigated under the specific conditions of the pulse radiolysis studies. Accordingly, in a first set of experiments all deuterated compounds were submitted to a deacetylation procedure previously developed in our laboratory. Briefly, the indoles were dissolved in acetone, added to 0.025 M Na_3PO_4 (pH 12.3), and allowed to stand under an argon atmosphere over 1 min at room temperature. ^{1}H NMR and MS analysis of the deacetylated indoles eventually recovered by ethyl acetate extraction did not show detectable isotope loss. In other experiments, deacetylated deuterated 5,6-dihydroxyindoles were separately incubated in 0.05 M phosphate buffer pH 7.4 at room temperature under argon, and their deuterium content was periodically monitored by NMR. Whereas 4,7d_2-**1** proved to be fairly stable, loss of deuterium at the 3-position was observed in the case of 2,3,4,7d_4-**1** and 2,3d_2-**1** over ca. 30 min. These results indicated that deuterium at the 2-, 4-, and 7-positions was fully retained in deprotected 5,6-dihydroxyindoles under the most commonly encountered conditions in studies of melanin formation. Deuteration at the 3-position resulted in less stable isotope labeling unless care was taken to ensure very short contact times (e.g., <5 min) with neutral aqueous media of natural isotope composition. All deuterated compounds were however stable when stored dry in the cold.

Pulse Radiolysis. Although already reported in previous papers,[7,19] pulse radiolysis experiments for **1**−**3** were repeated herein under identical conditions to allow for reliable comparison of data (full sets of new traces are provided as SI). All indole substrates were obtained in situ by the above-described deacetylation procedure, and deprotected 5,6-dihydroxyindoles (0.15 mM) were immediately subjected to pulse radiolysis. Generation of the oxidizing species $Br_2^{-\bullet}$ was achieved by irradiating N_2O-saturated solutions of 0.5 M KBr, and $Br_2^{-\bullet}$ radicals are formed within 0.1 μs after the radiation pulse according to the following equations:

$$H_2O \rightarrow e^-_{aq} + OH^\bullet \quad (2)$$

$$e^-_{aq} + N_2O + H_2O \rightarrow OH^\bullet + N_2 + OH^- \quad (3)$$

$$OH^\bullet + Br^- \rightarrow OH^- + Br^\bullet \quad (4)$$

$$Br^\bullet + Br^- \rightarrow Br_2^{-\bullet} \quad (5)$$

In this sequence, the highly reactive $Br_2^{-\bullet}$ radical serves as the main oxidant since, as produced, the first formed $OH^\bullet$ is rapidly scavenged by the excess Br^- in the medium. $Br_2^{-\bullet}$ reacts with the various 5,6-dihydroxyindoles at very fast rate, e.g., the estimated rate constant for the reaction with **1** was $k = 1.8 \times 10^9$ M^{-1} s^{-1}, and similar values were determined with all other substrates investigated.[25] These reactions are believed to proceed via a one-electron oxidation mechanism.[26] The first transient spectra were recorded at such a time that the buildup of initial radical absorption was complete and that subsequent decay had not proceeded to any significant extent, so they could be safely attributed to the semiquinones. A comparative view of the absorption traces of **1S**−**3S** (recorded at $t < 100$ μs) and their bimolecular decay products (recorded at $t > 800$ μs) is given in SI. All semiquinones decayed with formation of broad chromophores absorbing above 400 nm. Absorption properties and second-order decay rate constants $2k$ (M^{-1} s^{-1}) for **1S**−**3S** and deuterated **1S** are given in Table 1. **3S** decayed

Table 1. Absorption Maxima, Extinction Coefficients and Second-Order Decay Rate Constants for 1S−3S and Deuterated 1S

semiquinone	λ_{max} /nm (ε/M^{-1} cm^{-1})	second-order decay constant $2k/10^9$ M^{-1} s^{-1}
1S	490 (3400)	2.3 ± 0.08
2,3d_2-**1S**	490 (4000)	5.0 ± 0.12
4,7d_2-**1S**	490 (3400)	2.1 ± 0.08
2,3,4,7d_4-**1S**	490 (3600)	3.3 ± 0.10
2S	380 (11500)	1.3 ± 0.07
3S	500 (3240)	3.6 ± 0.10

at slightly faster rate than **1S**, while **2S** decayed more slowly, due probably to the stabilizing electronic factors or charge repulsion effects generated by the 2-carboxylate function.

Semiquinones from deuterium-substituted **1** displayed similar spectrophotometric behavior as the parent compound (see SI). However, 2,3d_2-**1S** and 2,3,4,7d_4-**1S** decayed at a significantly faster rate relative to **1S**, while 4,7d_2-**1** behaved like the parent indole. In such experiments great care was directed to minimize the contact time with the medium prior to pulse radiolysis experiments to limit as much as possible the deuterium loss from the 3-labeled derivative.

Overall, kinetic data in Table 1 revealed an unexpected site-specific inverse secondary isotope effect associated with deuterium labeling on the pyrrolic positions of the indole ring. Inverse secondary isotope effects are usually attributed to reaction pathways involving gradual conversion of sp^2-hybridized carbons of the reactant to a sp^3-type condition through quasi-tetrahedral transition-state geometries.[27,28] To the best of our knowledge, inverse secondary isotope effects are unprecedented in *ortho*-semiquinone decay. It is generally accepted that formation of dimeric products by one-electron oxidation of catechols involves disproportionation of the resulting semiquinone followed by a catechol-quinone coupling step (Scheme 3).

Since highly negative free energy changes usually characterize disproportionation equilibria, disfavoring accumulation of a significant concentration of semiquinone free radicals, the direct free radical coupling of *o*-semiquinones has never been considered as a viable route. In line with this view, a previous computational study showed that dimerization of three isomeric semiquinone radicals is endothermic, at variance

dx.doi.org/10.1021/ja4067332 | J. Am. Chem. Soc. 2013, 135, 12142−12149

Scheme 3. Possible Pathways of Second-Order Decay of 1S[a]

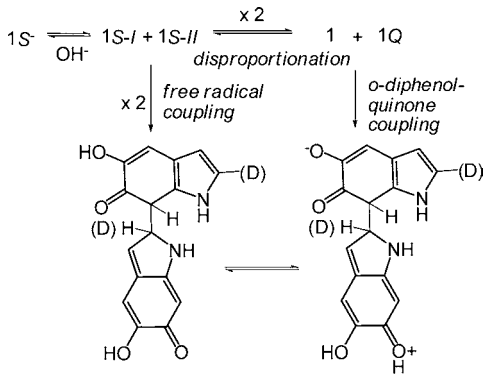

[a]The scheme shows conversion of the trigonal sp^2 C2 reactive site to a sp^3 geometry as determinant of the inverse isotope effect. For simplicity, only deuterium labeling at C2 is indicated.

with the self-coupling of the phenoxy radical which is exothermic.[29] In the case of 5,6-dihydroxyindoles, however, the observed inverse isotope effect suggested a rate-determining dimerization step. This observation, coupled with the failure to identify 5,6-indolequinone **1Q** in the pulse radiolysis experiments,[21] prompted a detailed re-examination of the various possible reaction pathways involved in the second-order decay of **1S**, with a view to identifying the actual rate-determining step.

Product Characterization. Direct investigation of the semiquinone decay products in the pulse radiolysis experiments was difficult due to the low substrate concentrations and the limited amounts of sample subjected to oxidation. Accordingly, model experiments were devised in which one-electron oxidation of **1** was carried out under conditions similar to those adopted in the pulse radiolysis reactions. Potassium ferricyanide was selected as the oxidant because of its mild reactivity and established one-electron mechanism.[30] After several trials, optimized conditions for product analysis were set up, involving oxidation of 1.5×10^{-4} M **1** with equimolar $K_3Fe(CN)_6$ for very brief reaction times (<30% substrate consumption) to prevent extensive melanization and loss of dimers. Under such conditions, the reaction led to complex pattern of products, all in minute amounts, which were analyzed by LC-MS after extraction and acetylation to prevent oxidative degradation.

Quite surprisingly, inspection of the LC-MS traces showed the exclusive formation of dihydrobiindole derivatives, but not of the fully aromatic dimers previously isolated by peroxidase/H_2O_2 oxidation.[18] Two of these products could be unambiguously identified as **4** and **5** (as the pentaacetyl derivatives) by comparison with unpublished samples isolated in a previous study (see SI).[6] Characteristic features of the ^{1}H NMR spectra of acetylated **4** and **5** were three distinct double doublets in the range of δ 3−6 indicative of the $-CH_2-CH<$ moiety on the reduced 2-substituted indoline ring.

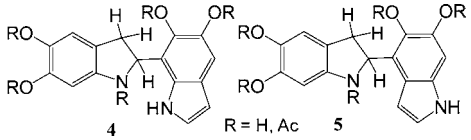

Dihydrobiindoles **4** and **5** conceivably arise by either of the coupling pathways in Scheme 3, after the fast re-aromatization of the substituted benzenoid ring and reduction of the 2-substituted moiety. The latter step can likely be attributed to redox exchange with the excess **1** in the reaction medium. Besides the reduced dimers, product analysis revealed reduced trimers and higher oligomers of **1** (not shown), which, together with insoluble eumelanin-like material, would account for the overall mass balance for reacted **1**.

Chromophore Analysis. To complete product characterization, the chromophores of the sp^3-biindole coupling products were analyzed at the DFT level of theory, and the results were compared with the absorption profiles of the pulse radiolytically generated second-order decay products of **1S**. Since most dimers comprise a 2-linked unit, absorption properties that included those of the 2*H*-tautomers of **1** were considered for all coupling products (see Scheme 3). All structures were geometry optimized at the DFT level, with a hybrid functional (PBE0)[31] and a reasonably large basis set [6-31+G(d,p)], and for each species, different tautomers/conformers were explored. Computations were performed either in vacuo or by adoption of a polarizable continuum medium (PCM)[32−34] to account for the influence of the aqueous environment. In view of the faster convergence, a scaled van der Waals cavity based on universal force field (UFF)[35] radii was used, and polarization charges were modeled by spherical Gaussian functions;[36,37] nonelectrostatic contributions to the solvation free energy were disregarded. The absorption spectra of all significant species were simulated both in vacuo and in water at the TD-DFT level[38,39] using the large 6-311++G(2d,2p) basis set. The computational levels chosen have been validated in a number of previous studies, in particular for what concerns energies and low-lying electronic transitions.[40−48] All calculations were performed with the Gaussian package.[49]

The simulated absorption spectra of the 2,4′- and 2,7′-coupling products (but not of the 2,2′-coupling product) displayed distinct maxima above 400 nm, in good agreement with the experimentally determined absorption properties of the decay products of **1S** under pulse radiolysis conditions. As apparent from the spectrophotometric changes accompanying decay of **1S** (top panel in Figure 1), the relatively intense band around 510 nm is gradually replaced by a broad and less defined absorption profile which, though likely due to mixtures of species, reveals a distinct rise at ca. 420 nm. This latter feature is the signature of the visible coupling products that are generated by decay of **1S**. Complete simulated absorption spectra and relevant transitions with oscillator strengths for all tautomers/conformers of putative coupling products of **1S** are given as SI.

On this basis, it can be suggested that the visible chromophores generated by second-order decay of **1S** under pulse radiolysis conditions reflect the generation of a mixture of free radical coupling products of the type shown in Scheme 3 and that these products have relatively long lifetimes, exceeding the ms time scale.

DFT Investigation of Semiquinone Disproportionation Equilibria. Since neither product analysis nor the inverse kinetic isotope effect per se did provide conclusive information about the actual dimerization pathway, a systematic computational analysis of the catechol-quinone coupling vs *o*-semiquinone self-coupling pathways depicted in Scheme 3 was undertaken. Preliminarily, the thermodynamics of disproportionation of semiquinones **1S**−**3S** were investigated by DFT calculations. Geometry optimizations were carried out as

dx.doi.org/10.1021/ja4067332 | J. Am. Chem. Soc. 2013, 135, 12142−12149

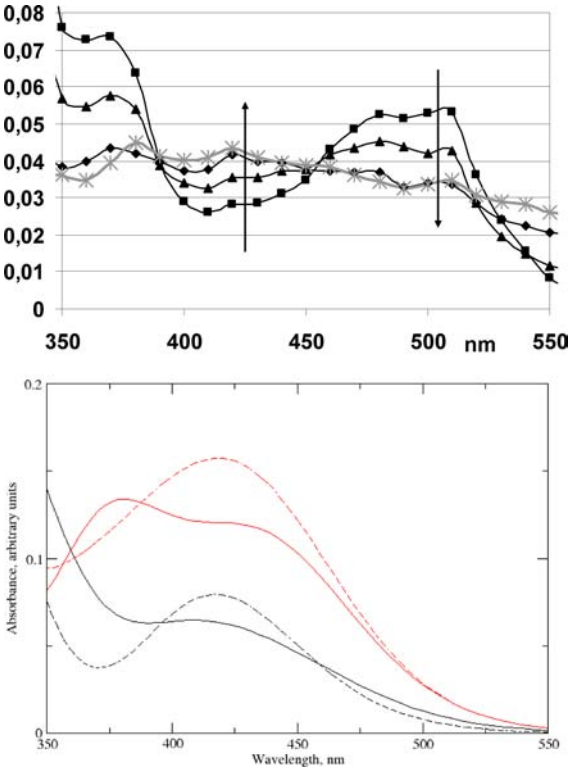

Figure 1. Experimental and computed absorption spectra of second-order decay products of **1S**. The top panel shows the absorption traces of the second-order decay product(s) of **1S** as recorded at 28 (■), 104 (▲), 510 (◆), and 882 (*) μs. The bottom panel reports the simulated UV−vis spectra of the most stable computed conformers of the 2,4′- and 2,7′-coupling products of **1S** as in Scheme 3; full black line, (2*RS*,7′*RS*)-2,7′-dimer, G+ conformer; dashed black line, (2*RS*,7′*SR*)-2,7′-dimer, T conformer; full red line, (2*RS*,4′*SR*)-2,4′-dimer, G+ conformer; dashed redline, (2*RS*,4′*RS*)-2,4′-dimer, G− conformer.

described above, either in vacuo or in water (PCM); in this case, nonelectrostatic terms were accounted for in single-point PCM calculations employing radii and nonelectrostatic terms of the SMD solvation model.[50] Vibrational−rotational contributions to the free energy were also calculated (at 298.15 K, in the rigid rotor harmonic oscillator approximation). In all cases, single point energy evaluations were then performed with the M062X functional.[51] Dispersion contributions[52] were estimated by single-point calculations employing the published M062X parametrization.[53] Finally, CBS-QB3[54] and CBS-APNO[55] calculations were carried out in selected cases for comparison. Computational results for the starting indoles **1**−**3**, semiquinone, and quinone intermediates and their tautomeric forms (geometries, energies, free energies) are reported in the SI.

DFT analysis of the possible isomers of neutral semiquinone radicals **1S**−**3S** predicted the 6-OH derived phenoxyl radicals (of the type **1S-I**) as the favored neutral species both in vacuo and in water, while the 5-OH derived radicals (of the type **1S-II**) were destabilized by ca. 2 kcal mol^{-1}. This difference can be explained considering that in **I**, but not in **II**, the odd electron may be efficiently delocalized to the pyrrole ring, as it can also be appreciated on inspection of simple resonance structures. Considering a pK_a value for the 6-OH group of **1S** of 6.8,[18,20] a significant contribution of anionic forms of semiquinones would be anticipated at pH 7.4. This contribution was assessed by investigation of the ionized species of **1S** as a representative semiquinone (see SI). Calculations of absorption spectra for both the neutral and anionic species supported the identity of the initially generated species as the semiquinones.

In line with previous results,[21] the computational analysis for the main tautomers of **1Q** indicated that the quinoneimine **1Q-III** is unstable and unlikely to contribute significantly to the product equilibrium composition. The quinone methide **1Q-II**, which is less stable in water than the *o*-quinone **1Q-I** by several kcal mol^{-1}, becomes closer in energy to the latter in vacuo, due probably to intramolecular OH···O hydrogen bonding. As previously reported,[21] simulated absorption spectra of *o*-quinones **1Q**−**3Q** did not reveal any significant transition above 400 nm (see SI).

The energy balances for the disproportionation reaction (eq 1), referred to the most stable tautomers/conformers identified for semiquinones and quinones from **1**−**3**, are reported in Table 2 (all values in kcal mol^{-1}).

Table 2. Calculated Balances for the Disproportionation Reaction of Semiquinones from 5,6-Dihydroxyindoles 1−3, Hydroquinone, and Catechol, Referred to the Most Stable Tautomers/Conformers Identified at Each Oxidation Level

substrate	$\Delta_{rxn}E_{vac}$/kcal mol^{-1}[a]	$\Delta_{rxn}G^{\circ}_{water}$/kcal mol^{-1}[b]
1	0.5 (2.8;[c] 0.4;[d] 1.3[e])	−4.2
2	−1.4[f]	−4.0
3	1.0	−3.8
hydroquinone	−24.3 (−25.5;[c] −26.6;[d] −26.4[e])	−15.1
catechol	−6.9 (−7.9;[c] −8.5[e])	−11.9

[a]Electronic energy at the M062X/6-31+G(d,p) level. [b]Estimated Gibbs free energy in water: RRHO Gibbs free energy at the M062X/6-31+G(d,p)/SMD level (including nonelectrostatic contributions) + empirical dispersion contribution. [c]CBS-QB3. [d]ROCBS-QB3. [e]CBS-APNO. [f]PCM free energy at the M062X/6-31+G(d,p) level.

The results revealed that free energy changes for disproportionation of semiquinones **1S**−**3S** are unexpectedly small. The possible dissociation of the phenolic OH groups was not explicitly addressed in this set of calculations. However, the pK_a value of 6.8 determined for **1S**[20,56] would suggest that this dissociation process may be operative and may induce an even larger shift of the disproportionation equilibrium toward the radicals.

To assess the reliability of the DFT data, similar calculations were performed for both *o*- and *p*-benzosemiquinone, for which information on thermodynamic parameters is available.[1] Much larger negative (free) energy changes were determined in both cases, in line with experimental evidence, supporting the value of the computational approach. Thus, from the thermodynamic viewpoint, the main conclusion from the data in Table 2 is that the disproportionation equilibrium for 5,6-dihydroxyindole semiquinones is less favorable than for other semiquinones, suggesting that a more significant concentration of semiquinone free radicals may be available for the self-coupling route. Based on these considerations, characterization of main bimolecular decay route of **1S** was sought by determining both ΔG values and the relative heights of the barriers expected for self-coupling of **1S** and for reaction of 1 with **1Q**, as in Scheme 3.

DFT Investigation of Free Energy Changes and Transition-State Barriers for Different Coupling Pathways. The energetics of catechol-quinone coupling of **1** with

dx.doi.org/10.1021/ja4067332 | J. Am. Chem. Soc. 2013, 135, 12142−12149

1Q, as well as of free radical self-coupling of **1S**, were computed for the representative 2,7′-coupling mode and for different protonation states of the reagents. Both coupling reactions involve the generation of intermediates with sp^3-carbons at the bonding sites. Such intermediates possess two stereogenic centers, leading potentially to two diastereoisomeric *dl* couples. Rotation around the newly formed sp^3−sp^3 C−C bond implies the existence of several (typically three) rotamers for each dimer species. Table 3 reports the minimum values of the free energy (kcal mol^{-1}) of the covalent dimers and of the transition structures, as referred to the corresponding values for the starting monomers.

Table 3. Computed energetics of 2,7′-coupling reactions of 1

no.	coupling species	coupling mode	$\Delta_{rxn}G^\circ_{water}$/ kcal mol^{-1}[a]	$\Delta^{\ddagger}G^\circ_{water}$/ kcal mol^{-1}
	1S (Free Radical) Self-Coupling			
1	O6-centered neutral **1S**	(2*RS*,7′*SR*), T	−8.7	5.7
2	radical anions $\mathbf{1S}^-$	(2*RS*,7′*RS*), G+	2.9	18.9
3	radical anion $\mathbf{1S}^-$ (2-position) + O6-centered neutral **1S** (7-position)	(2*RS*,7′*RS*), G+	−4.3	9.8
4	O6-centered neutral **1S** (2-position) + radical anion $\mathbf{1S}^-$ (7-position)	(2*RS*,7′*SR*), T	−2.0	10.3
	1-1Q (Catechol-Quinone) Coupling			
5	**1** (2-position) + **1Q** (7-position)	(2*RS*,7′*SR*), T	15.2	20.4
6	O6-deprotonated **1** (2-position) + **1Q** (7-position)	(2*RS*,7′*SR*), T	−3.5	8.8

[a]Estimated Gibbs free energy in water: RRHO Gibbs free energy at the M062X/6-31+G(d,p)/SMD level (including nonelectrostatic contributions) + empirical dispersion contribution; corrected to standard state concentrations of 1 M (see, e.g., ref 57).

Calculated ΔG values for free radical coupling of **1S** proved to be consistently negative, fully supporting the feasibility of the process on thermodynamic grounds. Less favorable changes were predicted with the negatively charged forms of **1S**. Conversely, a relatively high ΔG value was computed for the **1-1Q** coupling path, due to formation of an unstable zwitterion as first intermediate. The balance is however reverted by inclusion of a charged catecholate species.

Inspection of free energy values for the transition structures along the coupling pathways revealed a much higher barrier for the **1-1Q** coupling (no. 5) relative to the free radical self-coupling of **1S** (no. 1). Even if a catecholate is included in the catechol-quinone coupling pathway (no. 6), the computed barrier remains comparatively high. From these data, predicted second-order rate constants were 4.1×10^8 M^{-1} s^{-1} for the free radical self-coupling of **1S** (no. 1), 6.8×10^{-3} M^{-1} s^{-1} for the **1-1Q** coupling reaction (no. 5), and 2.2×10^6 M^{-1} s^{-1} for the catecholate-quinone pathway.

Decay Mechanism of 1S. A purposeful mechanistic analysis from the data in Table 3 requires consideration of the relative concentrations of the various neutral, ionic, and free radical species under the specific conditions of the pulse radiolysis experiments. In a typical experimental condition, the maximum concentration of **1S** ($QH^\bullet$ in eq 1) that builds up right after pulse radiolysis can be estimated as 5.0×10^{-6} M, based on a molar absorptivity of 3400 M^{-1} cm^{-1}.[5,19] Unreacted **1** (QH_2 in eq 1) is present in a large excess (ca. 1.5×10^{-4} M), and its concentration may therefore be taken as being virtually constant during the whole reaction course.

The data in Table 2 imply an equilibrium constant $K_{eq} = 1.2 \times 10^3$ for the disproportionation reaction: 2 **1S** → **1** + **1Q**. If one further takes into account the deprotonation equilibrium of **1S** to $\mathbf{1S}^-$, one can compute an upper limit for the concentration of **1Q** (i.e., the concentration attainable if the disproportionation reaction would actually reach equilibrium) of 1.9×10^{-6} M.

Putting now the above calculated rate constants and estimated concentrations into second-order rate laws, the following reaction rates for competing dimerization processes nos. 1 and 5 (Table 3) can be estimated:

$$v(\#1) = 9.6 \times 10^{-5} Ms^{-1}$$

$$v(\#5) = 1.9 \times 10^{-12} Ms^{-1}$$

$$v(\#6) = 7.7 \times 10^{-6} Ms^{-1}$$

It could be concluded that, under pulse radiolysis conditions, free radical coupling would be by far the dominant route of bimolecular decay of **1S**.

A semiquinone coupling pathway leading to a 2,2′-biindole in the tautomeric form was postulated in a previous theoretical study.[21] This suggestion was based on relative energy data in which the 2*H*-quinone methide was predicted to be the most stable minor tautomer of **1**, differing from the parent catechol by only 3.9 kcal mol^{-1} in vacuo. Notably, in the same study the calculated electronic transitions for the 2*H*-quinone methide moiety of the proposed dimerization product in Scheme 3 were shown to fall in the range 370−420 nm, i.e., the same range where a distinct absorption band is observed in the pulse radiolysis experiments.

The free radical coupling pathway in Scheme 3 would also be consistent with the observed site specificity of the kinetic isotope effects at C2, a conclusion supported by product distribution. The lack of effect on the 4,7-dideuterated derivative is unclear and could be taken to suggest the dominant formation of the 2,2′-biindole, but this was difficult to demonstrate. It is also possible that the observed difference in isotope effects reflects different degrees of conversion of the trigonal sp^2 carbons to the sp^3 geometry at the various reactive sites. All these issues require verification.

Further assessment of the viability of the free radical coupling mechanism illustrated in Scheme 3 required computational investigation of transition-state features that would justify an inverse secondary kinetic isotope effects. This issue could not be extensively addressed in the present paper because of the most demanding systematic exploration of transition states required by theoretical analysis of secondary isotope effects. In the case of **1S**, complexity arises from the various possible modes of coupling, e.g., via 2,2′-, 2,4′-, or 2,7′-bondings. Moreover, for each coupling mode two diastereoisomers of the first formed sp^3 coupling products must be considered, entailing in turn several conformers.

Nonetheless, for the purposes of this study, a preliminary analysis of the transition states along the representative 2,7′-coupling route of the O6-centered form of **1S** (neutral form) was carried out, in comparison with the analogous catechol-quinone 2,7′-coupling pathway. The results reported in Table 4 consistently predicted an inverse secondary kinetic isotope effect for the deuterated derivatives in both cases.

A more detailed computational analysis is necessary to improve the matching of predicted k_H/k_D values with the experimental data in Table 1.

Table 4. Computed Kinetic Isotope Effects for 2,7′-Dimerization of 1S-I (Neutral Forms in Water) and 1-1Q (Neutral Forms in Water As Well As O6-Deprotonated 1 + 1Q in Water)[a]

coupling species	coupling mode	$\Delta\Delta^{\ddagger}G^{\circ}_{water}$ /kcal mol^{-1}	k_H/k_D
1S (free radical) self-coupling			
O6-centered neutral **1S**	(2*RS*,7′*SR*), T	−0.106	0.84
1-1Q (catechol-quinone) coupling			
1 (2-position) + **1Q** (7-position)	(2*RS*,7′*SR*), T	−0.156	0.77
O6-deprotonated **1** (2-position) + **1Q** (7-position)	(2*RS*,7′*SR*), T	−0.129	0.80

[a]Changes in activation free energy (in kcal mol^{-1}, for paths through the most favorable transition structures: see Supplementary information) issuing from 2,3,4,7d_4 monomer substitution and corresponding computed kinetic isotope effects are reported.

CONCLUSIONS

It was previously shown by pulse radiolysis experiments that 5,6-dihydroxyindole semiquinones decay by a second-order pathway and generate visible absorbing species that were not compatible with 5,6-indolequinones produced via a disproportionation mechanism. Herein, we re-examined the pulse radiolysis behavior of 5,6-dihydroxyindole semiquinones using deuterium-labeled derivatives and revisited the fate of semiquinones by a detailed DFT investigation combined with product characterization. Altogether, the results showed that: (a) Bimolecular decay of **1S** is susceptible to a significant inverse isotope effect specifically associated to indole labeling at C2; (b) one-electron oxidation of **1** with potassium ferricyanide under conditions mimicking the pulse radiolysis experiments led to the formation of dihydrobiindole species probably via reduction of sp^3-coupled biindole intermediates; (c) the simulated absorption spectra of the sp^3 biindole intermediates generated by free radical coupling products were in good agreement with the observed absorption properties of the species produced by pulse radiolysis oxidation of **1**; (d) small negative ΔG values for the disproportionation of semiquinones **1S**−**3S** were predicted, suggesting that significant concentrations of semiquinones **1S**−**3S** may be present under equilibrium conditions favoring coupling; and (e) predicted reaction rates for the free radical coupling of **1S** were 1 order of magnitude faster than those predicted for **1-1Q** coupling due to much lower transition state barriers.

These integrated sets of experimental and computational data concurred to suggest that semiquinones **1S**−**3S** decay mainly by a free radical dimerization pathway, thus explaining the chromophoric phases observed during pulse radiolysis oxidation. To the best of our knowledge, this is the first study reporting a free radical coupling of semiquinones, thus pointing to a revisitation of the mechanisms of 5,6-dihydroxyindole polymerization. Okuda et al.[58] recently addressed the mechanism of oxidative dimerization of **1**. Using a general-purpose reactivity indicator derived from ab initio DFT calculations, they concluded that four conformers of **1** may participate in the reaction as a nucleophile, while **1Q** predominantly participates as an electrophile among three tautomers. Based on the present data, a more complex picture of 5,6-dihydroxyindole dimerization is proposed in which an interplay of semiquinone radicals and quinone products generated by the disproportionation equilibrium would render both indole/quinone and free radical coupling routes possible. In this regard, 5,6-indolequinone intermediates have been demonstrated by trapping with nucleophilic sulfur compounds, e.g., thiouracil.[59] It should be emphasized that the present study does not take into account the involvement of other factors present in a biological microenvironment, so the relevance to eumelanin synthesis in vivo remains to be assessed. It is possible that redox exchange mechanisms with quinones, thiols, or other ingredients of the cellular milieu affect 5,6-dihydroxyindole oxidation driving the disproportionation equilibrium toward either of the competing pathways.

As a final remark, it is worth noting that free energy balances for disproportionation processes similar to those of **1S** were predicted for 2,3-dihydroxynaphthalene semiquinone (see SI). These results would point to a broader relevance of semiquinone free radical coupling than formerly believed, possibly associated to specific *o*-dihydroxylation patterns on bicyclic ring systems destabilizing the corresponding *o*-quinones.

Assessment of the actual relevance and scope of semiquinone free radical coupling is expected to stimulate a profound revision of current notions and views about semiquinone chemistry.

ASSOCIATED CONTENT

Supporting Information

Experimental procedures and spectroscopic data for all new compounds S1, ^{13}C and ^{15}N CP MAS and spectra of reference compounds, NMR data and LDI-MS tables. This material is available free of charge via the Internet at http://pubs.acs.org.

AUTHOR INFORMATION

Corresponding Author

vincenzo.barone@sns.it; dischia@unina.it

Notes

The authors declare no competing financial interest.

ACKNOWLEDGMENTS

This work was carried out with financial support from Italian MIUR PROxi project (PRIN 2010-2011 prot. 2010PFLRJR to MdI; PRIN 2010-2011 prot. 2010FM738P_002 to OC), within the aims of the EuMelaNet special interest group of the European Society for Pigment Cell Research (http://www.espcr.org/eumelanet/).

REFERENCES

(1) Alegria, A. E.; Lopez, M.; Guevara, N. *J. Chem. Soc., Faraday Trans.* **1996**, *92*, 4965−4968.
(2) Roginsky, V. A.; Pisarenko, L. M.; Bors, W.; Michel, C.; Saran, M. *J. Chem. Soc., Faraday Trans.* **1998**, *94*, 1835−1840.
(3) Kalyanaraman, B.; Felix, C. C.; Sealy, R. C. *Environ. Health Perspect.* **1985**, *64*, 185−198.
(4) Asher, J. R.; Doltsinis, N. L.; Kaupp, M. *J. Am. Chem. Soc.* **2004**, *126*, 9854−9861.
(5) Pezzella, A.; Panzella, L.; Crescenzi, O.; Napolitano, A.; Navaratnam, S.; Edge, R.; Land, E. J.; Barone, V.; d'Ischia, M. *J. Am. Chem. Soc.* **2006**, *128*, 15490−11221.
(6) Pezzella, A.; Panzella, L.; Natangelo, A.; Arzillo, M.; Napolitano, A.; d'Ischia, M. *J. Org. Chem.* **2007**, *72*, 9225−9230.
(7) Pezzella, A.; Panzella, L.; Crescenzi, O.; Napolitano, A.; Navaratnam, S.; Edge, R.; Land, E. J.; Barone, V.; d'Ischia, M. *J. Org. Chem.* **2009**, *74*, 3727−3734.
(8) Arzillo, M.; Pezzella, A.; Crescenzi, O.; Napolitano, A.; Land, E. J.; Barone, V.; d'Ischia, M. *Org. Lett.* **2010**, *12*, 3250−3253.

(9) Arzillo, M.; Mangiapia, G.; Pezzella, A.; Heenan, R. K; Radulescu, A.; Paduano, L.; d'Ischia, M. *Biomacromolecules* **2012**, *13*, 2379−2390.
(10) Reale, S.; Crucianelli, M.; Pezzella, A.; d'Ischia, M.; De Angelis, F. *J. Mass Spectrom.* **2012**, *47*, 49−53.
(11) Ito, S.; Wakamatsu, K.; d'Ischia, M.; Napolitano, A.; Pezzella, A. In *Melanins and Melanosomes*; Borovanský, J., Riley, P. A., Eds.; John Wiley & Sons: Hoboken, NJ, 2011, 167−185.
(12) Simon, J. D.; Peles, D.; Wakamatsu, K.; Ito, S. *Pigm. Cell Melanoma Res.* **2009**, *22*, 563−579.
(13) Simon, J. D.; Peles, D. N. *Acc. Chem. Res.* **2010**, *43*, 1452−1460.
(14) Prota, G.; d'Ischia, M.; Mascagna, D. *Melanoma Res.* **1994**, *4*, 351−358.
(15) d'Ischia, M.; Napolitano, A.; Pezzella, A.; Meredith, P.; Sarna, T. *Angew. Chem., Int. Ed.* **2009**, *48*, 3914−3921.
(16) Mostert, A. B.; Powell, B. J.; Pratt, F. L.; Hanson, G. R.; Sarna, T.; Gentle, I. R.; Meredith, P. *Proc. Natl. Acad. Sci. U.S.A.* **2012**, 1−5.
(17) Meredith, P.; Sarna, T. *Pigm. Cell Res.* **2006**, *19*, 572−594.
(18) d'Ischia, M.; Napolitano, A.; Pezzella, A.; Land, E. J.; Ramsden, C. A.; Riley, P. A. *Adv. Heterocycl. Chem.* **2005**, *89*, 1−63.
(19) Lambert, C.; Chacon, J. N.; Chedekel, M. R.; Land, E. J.; Riley, P. A.; Thompson, A.; Truscott, T. G. *Biochim. Biophys. Acta* **1989**, *993*, 12−20.
(20) Al-Kazwini, A. T.; O'Neill, P.; Adams, G. E.; Cundall, R. B.; Lang, G.; Junino, B. *J. Chem. Soc., Perkin Trans. 2* **1991**, 1941−1945.
(21) Il'ichev, Y. V.; Simon, J. D. *J. Phys. Chem. B* **2003**, *107*, 7162−7171.
(22) Pezzella, A.; Crescenzi, O.; Natangelo, A.; Panzella, L.; Napolitano, A.; Navaratnam, S.; Edge, R.; Land, E. J.; Barone, V.; d'Ischia, M. *J. Org. Chem.* **2007**, *72*, 1595−1603.
(23) Lista, L.; Pezzella, A.; Napolitano, A.; d'Ischia, M. *Tetrahedron* **2008**, *64*, 234−239.
(24) Wakamatsu, K.; Ito, S. *Anal. Biochem.* **1988**, *170*, 335−340.
(25) Edge, R.; d'Ischia, M.; Land, E. J.; Napolitano, A.; Navaratnam, S.; Panzella, L.; Pezzella, A.; Ramsden, C. A; Riley, P. A. *Pigm. Cell Res.* **2006**, *19*, 443−450.
(26) Land, E. J. *J. Chem. Soc., Faraday Trans.* **1993**, *89*, 803−810.
(27) Jones, W. D. *Acc. Chem. Res.* **2003**, *36*, 140−146.
(28) Parkin, G. *Acc. Chem. Res.* **2009**, *42*, 315−325.
(29) Alsoufi, A.; Altarawneh, M.; Dlugogorski, B. Z.; Kennedy, E. M.; Mackie, J. C. *J. Mol. Struct.: THEOCHEM* **2010**, *958*, 106−115.
(30) Terland, O.; Almås, B.; Flatmark, T.; Andersson, K. K.; Sørlie, M. *Free Radical Biol. Med.* **2006**, *41*, 1266−1271.
(31) Adamo, C.; Barone, V. *J. Chem. Phys.* **1999**, *110*, 6158−6169.
(32) Tomasi, J.; Mennucci, B.; Cammi, R. *Chem. Rev.* **2005**, *105*, 2999−3093.
(33) Cossi, M.; Scalmani, G.; Rega, N.; Barone, V. *J. Chem. Phys.* **2002**, *117*, 43−54.
(34) Scalmani, G.; Barone, V.; Kudin, K. N.; Pomelli, C. S.; Scuseria, G. E.; Frisch, M. J. *Theor. Chem. Acc.* **2004**, *111*, 90−100.
(35) Rappé, A. K.; Casewit, C. J.; Colwell, K. S.; Goddard, W. A., III.; Skiff, W. M. *J. Am. Chem. Soc.* **1992**, *114*, 10024−10035.
(36) York, D. A.; Karplus, M. *J. Phys. Chem. A* **1999**, *103*, 11060−11079.
(37) Scalmani, G.; Frisch, M. J. *J. Chem. Phys.* **2010**, *132*, 114110/1−114110/10.
(38) Bauernschmitt, R.; Ahlrichs, R. *Chem. Phys. Lett.* **1996**, *256*, 454−464.
(39) Casida, M. E.; Jamorski, C.; Casida, K. C.; Salahub, D. R. *J. Chem. Phys.* **1998**, *108*, 4439−4449.
(40) Jacquemin, D.; Wathelet, V.; Perpète, E. A. *J. Phys. Chem. A* **2006**, *110*, 9145−9152.
(41) Preat, J.; Jacquemin, D.; Wathelet, V.; André, J.-M.; Perpète, E. A. *J. Phys. Chem. A* **2006**, *110*, 8144−8150.
(42) Jacquemin, D.; Preat, J.; Wathelet, V.; Fontaine, M.; Perpète, E. A. *J. Am. Chem. Soc.* **2006**, *128*, 2072−2083.
(43) Barone, V.; Polimeno, A. *Chem. Soc. Rev.* **2007**, *36*, 1724−1731.
(44) Barone, V.; Improta, R.; Rega, N. *Acc. Chem. Res.* **2008**, *41*, 605−616.
(45) Barone, V.; Baiardi, A.; Biczisko, M.; Bloino, J.; Cappelli, C.; Lipparini, F. *Phys. Chem. Chem. Phys.* **2012**, *14*, 12404−12422.
(46) Crescenzi, O.; Pavone, M.; De Angelis, F.; Barone, V. *J. Phys. Chem. B* **2005**, *109*, 445−453.
(47) Aquilante, F.; Cossi, M.; Crescenzi, O.; Scalmani, G.; Barone, V. *Mol. Phys.* **2003**, *101*, 1945−1953.
(48) Adamo, C.; Barone, V. *Chem. Phys. Lett.* **2000**, *330*, 152−160.
(49) Frisch, M. J.; Trucks, G. W.; Schlegel, H. B.; Scuseria, G. E.; Robb, M. A.; Cheeseman, J. R.; Scalmani, G.; Barone, V.; Mennucci, B.; Petersson, G. A.; Nakatsuji, H.; Caricato, M.; Li, X.; Hratchian, H. P.; Izmaylov, A. F.; Bloino, J.; Zheng, G.; Sonnenberg, J. L.; Hada, M.; Ehara, M.; Toyota, K.; Fukuda, R.; Hasegawa, J.; Ishida, M.; Nakajima, T.; Honda, Y.; Kitao, O.; Nakai, H.; Vreven, T.; Montgomery, J. A., Jr.; Peralta, J. E.; Ogliaro, F.; Bearpark, M.; Heyd, J. J.; Brothers, E.; Kudin, K. N.; Staroverov, V. N.; Kobayashi, R.; Normand, J.; Raghavachari, K.; Rendell, A.; Burant, J. C.; Iyengar, S. S.; Tomasi, J.; Cossi, M.; Rega, N.; Millam, J. M.; Klene, M.; Knox, J. E.; Cross, J. B.; Bakken, V.; Adamo, C.; Jaramillo, J.; Gomperts, R.; Stratmann, R. E.; Yazyev, O.; Austin, A. J.; Cammi, R.; Pomelli, C.; Ochterski, J. W.; Martin, R. L.; Morokuma, K.; Zakrzewski, V. G.; Voth, G. A.; Salvador, P.; Dannenberg, J. J.; Dapprich, S.; Daniels, A. D.; Farkas, Ö.; Foresman, J. B.; Ortiz, J. V.; Cioslowski, J.; Fox, D. J. *Gaussian 09*, revision A.1; Gaussian, Inc.: Wallingford, CT, 2009.
(50) Marenich, A. V.; Cramer, C. J.; Truhlar, D. G. *J. Phys. Chem. B* **2009**, *113*, 6378−6396.
(51) Zhao, Y.; Truhlar, D. G. *Theor. Chem. Acc.* **2008**, *120*, 215−241.
(52) Grimme, S.; Antony, J.; Ehrlich, S.; Krieg, H. J. *Chem. Phys.* **2010**, *132*, 154104.
(53) Goerigk, L.; Grimme, S. *Phys. Chem. Chem. Phys.* **2011**, *13*, 6670−6688.
(54) Montgomery, J. A., Jr.; Frisch, M. J.; Ochterski, J. W.; Petersson, G. A. *J. Chem. Phys.* **2000**, *112*, 6532−6542.
(55) Ochterski, J. W.; Petersson, G. A.; Montgomery, J. A., Jr. *J. Chem. Phys.* **1996**, *104*, 2598−2619.
(56) Al-Kazwini, A. T.; O'Neill, P.; Adams, G. E.; Cundall, R. B.; Jacquet, B.; Lang, G.; Junino, A. *J. Phys. Chem.* **1990**, *94*, 6666−6670.
(57) Cramer, C. J. *Essentials of Computational Chemistry: Theories and Models*, 2nd ed.; John Wiley & Sons: Chichester, 2004, pp 378−379.
(58) Okuda, H.; Wakamatsu, K.; Ito, S.; Sota, T. *J. Phys. Chem. A.* **2008**, *112*, 11213−11222.
(59) Napolitano, A.; Palumbo, A.; d'Ischia, M.; Prota, G. *J. Med. Chem.* **1996**, *39*, 5192−5201.